Supplementary Information

Porous Hierarchically Ordered Hydrogels Demonstrating Structurally Dependent Mechanical Properties

Elisabeth C. Lloyd,[1] Sujata Dhakal,[2] Shahrouz Amini,[3] Rami Alhasan,[4] Peter Fratzl,[3] Douglas R. Tree,[4] Svetlana Morozova,[2] Robert J. Hickey[1,5,*]

[1]Materials Science and Engineering, The Pennsylvania State University, University Park, PA 16802, USA
[2]Macromolecular Science and Engineering, Case Western Reserve University, Cleveland, OH 44106, USA
[3]Max Planck Institute of Colloids and Interfaces, Department of Biomaterials, Research Campus Golm, 14424 Potsdam, Germany
[4]Chemical Engineering, Brigham Young University, Provo, UT 84602, USA
[5]Materials Research Institute, The Pennsylvania State University, University Park, PA 16802, USA

*Corresponding author: rjh64@psu.edu

Table of Contents

Supplementary Methods

1. Synthesis and Characterization of Block Copolymers

The triblock copolymer, poly(styrene)-poly(ethylene oxide)-poly(styrene) (SOS) used in this study was synthesized using sequential living anionic polymerization.[1] Briefly, styrene (Sigma-Aldrich) monomer was first freeze-pump-thawed and then purified twice over di-*n*-butylmagnesium (Sigma-Aldrich, 1.0 M in heptane). Purified styrene monomer was then initiated using *sec*-butyllithium (Sigma-Aldrich, 1.4 M in cyclohexane), functionalized with ethylene oxide (Sigma-Aldrich, ≥ 99.5%) after 4 h, and finally terminated with methanol to produce the hydroxyl-terminated S homopolymer,[2] which was then precipitated in methanol and dried under vacuum. The purified S homopolymer was re-dissolved in tetrahydrofuran (THF) and re-initiated with potassium naphthalenide.[3] Potassium naphthalenide was prepared by adding a 3.6 molar excess of naphthalene with respect to potassium metal in a 250 mL round bottom flask and then adding THF to make a 0.2 M solution. The naphthalene/potassium metal THF solution was mixed for 24 h before using in the re-initiation of S. Ethylene oxide monomer, purified twice over *n*-butyllithium solution (Sigma-Aldrich, 1.6 M in hexanes), was then added to the reactor to form the SO diblock. A 20 mL aliquot was taken from the reactor after 24 h and terminated in sparged methanol.

After removal of the aliquot, the SOS triblock was formed by coupling the SO diblock with α,α′-dibromo-*p*-xylene (Sigma-Aldrich, 97%).[1] 10 mL of a supersaturated, air-free solution of cesium iodide (Sigma-Aldrich, 99.9%) in THF, stirred overnight at 45 °C, was added prior to the coupling agent as a source of counterions to reduce aggregation. An air-free solution of the coupling agent was similarly prepared, and the molar equivalence of one-half the number of moles of S precursor was gradually added to the reactor over a period of 4 h using a syringe pump. After 24 h, any remaining diblock was terminated with sparged methanol and precipitated in a 1:3 mixture of isopropanol and hexane. The molecular weight values for the S precursor, the diblock

copolymer, and the triblock polymer as well as the individual block molecular weights, PEO volume fraction (f_O), and dispersity are listed in Table S1. The molecular weight of all synthesized polymers (e.g., S-OH, SO, and SOS) were measured using a Tosoh GPC equipped with a Wyatt multi-angle light scattering detector and THF as the mobile phase. The increase in molecular weight with each successive step of the reaction is shown in the decrease in elution time in Figure S1. The difference in the molecular weight between the SO diblock and S homopolymer determined the PEO block length, which was doubled to obtain the length of the PEO mid-block in the SOS triblock. The average molecular weight obtained from the SEC of the final tri-block sample is also listed. To ensure the dn/dc used in the calculations was correct, the volume fraction of PEO in the diblock and triblock samples was determined using H^1 NMR in deuterated chloroform.

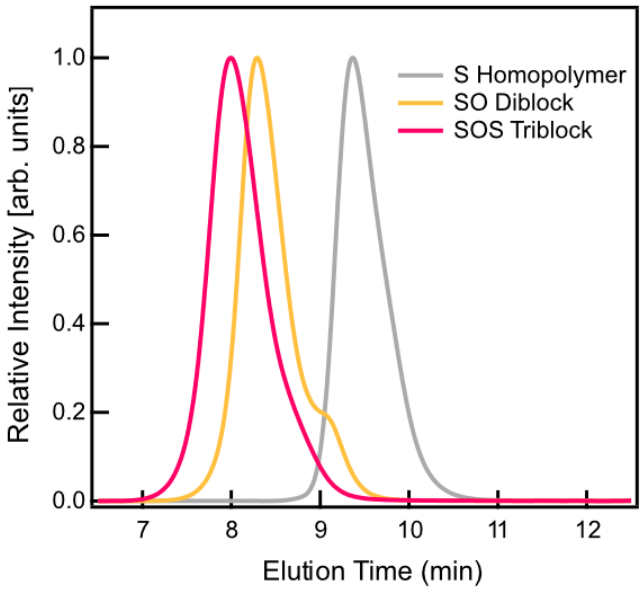

Figure S1. Size exclusion chromatography (SEC) traces for the synthesized polymers. There is an increase in polymer molecular weight as indicated in the decrease in elution time with successive living anionic polymerization steps: 1) S homopolymer (gray), 2) SO diblock copolymer (yellow), and 3) SOS triblock (magenta).

Table S1: Molecular characteristics of the polymers

Polymer	$M_{n,\,total}$[a] (kg/mol)	$M_{n,O}$[b] (kg/mol)	$M_{n,S}$[b] (kg/mol)	f_O[c]	$Đ$[d]
S (13)	13.1	-	13.1	-	1.04
SO (13-96)	118.2	96.2	13.1	0.90	1.04
SOS (13-192-13)	182.4	192.4	13.1	0.90	1.05

[a]Number-average molecular weight (M_n) of synthesized polymers were determined using SEC. For the S homopolymer, previously reported dn/dc values were used.[1] For copolymers, the dn/dc values were calculated from polymer block weight fractions determined from ^{1}H NMR. [b]M_n values of polymer blocks were calculated from $M_{n,total}$ and weight fraction of different blocks obtained from ^{1}H NMR. [c]The O block volume fraction (f_O) of the block copolymer was calculated using ^{1}H NMR data. The polymer block density values reported from Sigma-Aldrich, S is 1.04 g mL^{-1} and O is 1.13 g mL^{-1} at 25 °C, where used to calculate f_O. [d]Dispersity values ($Đ = M_w/M_n$) was determined from SEC.

2. Polymer Solution Viscosity Measurements

The viscosity of the initial polymer solutions in both THF and DMF were measured via flow sweep experiments in the 1 – 500 Hz range at room temperature using a Discovery HR-3 Hybrid Rheometer. Parallel plate geometries measuring 2 cm for entangled solutions and 6 cm for semi-dilute solutions were used to characterize viscosity (Figure S2a). A solvent trap, as well as 1 mL of the organic solvent at the top of the parallel plate geometry, was used to prevent the evaporation of the solvent, which was particularly important for THF samples at higher concentrations. Due to visible aggregates forming in the 11 and 12 wt% THF samples at high shear, stepwise steady shear measurements were also performed, with the average taken at each data point the overall average viscosity was then plotted with respect to concentration (Figure S2b).

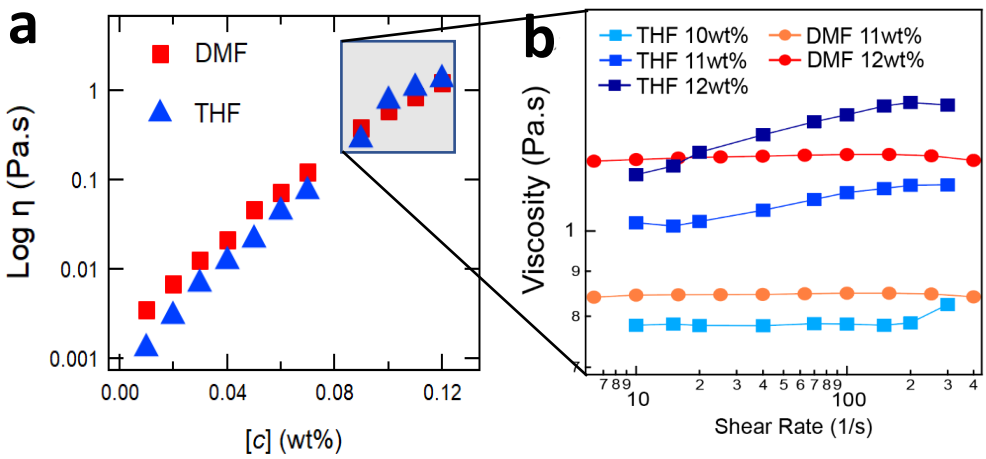

Figure S2. Polymer solution viscosity (η) versus concentration (c) for polymer solutions prepared using THF (blue) and DMF (red). Viscosity measurements were performed by taking the average of a flow sweep in the 5 – 500 Hz range. In the entangled regime, the viscosity of the solutions prepared using DMF and THF are similar, allowing the viscosity to be matched between two samples (shaded region).

The average viscosity from the raw data at each concentration was fit with a trendline to calculate the concentration required to match the viscosity of two samples at 1.0 Pa.s: THF 11.0 wt% and DMF 11.5 wt%. The relatively close match between the DMF and THF solutions in this regime allowed a minimal difference in concentration when matching viscosity.

3. Production of Hydrogels

a) Hierarchical Fibers from Injection

Initial solutions were prepared at concentrations of 11.0, 12.5, and 14.5 wt% in THF, and 9.5, 10.5, and 11.5 wt% in DMF. The solutions were stirred at 45 °C for a minimum of 3 h to ensure total dissolution before being injected into a syringe. To remove aggregates or bubbles that appeared as a result of the transfer from vial to syringe, the syringes were heated for several minutes under a stream of warm water, sealed in Parafilm© to prevent water from entering the syringe.

Solutions were injected using a 19-gauge needle with an inner diameter of 0.686 mm at a rate of 1.00 mL/min via a syringe pump. To prevent an appreciable reduction in the concentration gradient driving diffusion of the organic solvent, a minimum ratio of 1 L of water per 1 mL of injected solution was used in all cases. Due to the proximity to the surface and lower density of the organic solvents relative to water, tweezers were used to hold the end of the fibers below the surface for several seconds, at which point enough solvent had diffused out of the hydrogels to allow them to sink. Although the fibers formed immediately on injection into the water bath, they were left in the water bath for at a minimum of 1 h, at which point they were transferred to 20 mL scintillation vials for storage.

b) Hydrogels Prepared from Mold Immersion

The influence of shear on the formation of the hydrogel nanostructure was assessed by creating hydrogels in a mold and submerging them into a water bath. Hydrogels produced using a mold were thicker and less uniform as compared to the injected hydrogel fibers.

c) Conventional Physical Hydrogels as a Control

Conventional SOS triblock copolymer hydrogels were prepared using a modified procedure from Guo and Bailey[4] to compare to hydrogels created using rapid injection processing. The SOS polymer was placed in an aluminum 4-inch dog bone mold and thermally pressed into shape at 100 psi at 150 °C. After pressing, the polymer still in the mold was transferred to a vacuum oven and annealed at 150 °C for 24 h and then cooled to room temperature. Once at room temperature, the sample was immersed in water for 3 d. The prepared sample was then characterized via SAXS and oscillatory shear rheology for comparison with the hierarchically ordered hydrogels. A small piece of dry annealed polymer was also retained for characterization.

4. Hydrogel Swelling Ratio

The fraction of polymer contributing to the mass of the hydrogel fibers was determined by weighing the hydrogels in the hydrated and dry states and dividing the former by the latter. The hierarchical hydrogel fibers exhibit exceptionally high-water weight fractions compared with hydrogels prepared via conventional methods.[4] Furthermore, the hydrogel water weight fractions were surprisingly consistent with one another even with repetition, despite variations in the initial solution solvent and concentration, as well as hydrogel microstructure.

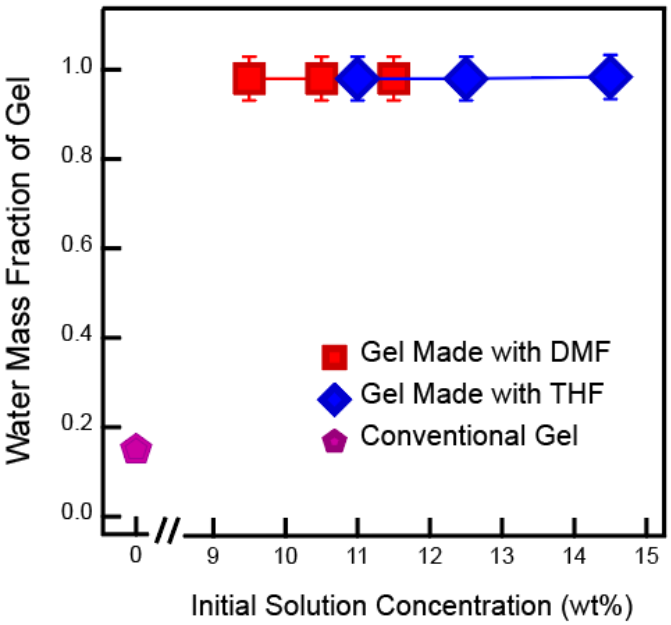

Figure S3. Measured water weight fractions of hierarchical hydrogels. Nearly all the DMF (red) and THF (blue) samples were 97.3% water by weight, with only the highest concentration of THF containing 97.7% water by weight. The water weight fraction of a SOS hydrogel prepared using conventional methods — as described in section 3a — is shown in pink. Water weight fractions for all samples are represented as mean values with error bars representing standard deviation. The number of replicate measurements are n = 3 with ± 0.02.

5. Small-Angle X-Ray Scattering Data

a. Data collection

Due to the high-water content of the hydrogels, a synchrotron source was required to obtain scattering data. Small-angle X-ray scattering (SAXS) measurements were performed at Brookhaven National Laboratory, National Synchrotron Light Source – II (NSLS – II), beamline 11-BM Complex Materials Scattering (CMS). The natural adhesion of the hydrogel fibers allowed them to remain in the grooves of capillary holders during measurements. Hydrogel fibers were folded over themselves to achieve better signal where necessary. Samples were exposed for 3 s using a 13.5 keV beam with a wavelength of 0.9184 Å. A sample to detector distance of 10 m was used to access the q-range 0.0044-0.03 $Å^{-1}$. 2D scattering patterns were obtained using a Pilatus 2M detector. An empty beam was used to subtract the background from the hydrogel and converted to a 1D plot of intensity versus q. The background subtraction and conversion were performed for every sample measured at the beamline using the program SciAnalysis (https://github.com/CFN-softbio/SciAnalysis). The 1D scattering data and fits are shown for hydrogels of all concentrations for both solvents (Figure 2b).

b. In Situ SAXS Under Extension

The effect of uniaxial extension on hydrogel nanostructure was explored using in situ SAXS measurements. Samples were placed in a Linkam Modular Force Stage with Kapton windows mounted in the beam path and strained at a rate of 3/min — the same as in all mechanical property characterizations — to 1x, 2x, 3x, and 4x their initial length, consecutively. At each extension, the sample was held in place and exposed for 3 s using a 13.5 keV beam with a wavelength of 0.9184 Å. Higher extensions could not be accessed due to the decreasing diameter of the gel fibers and the damage caused by the X-ray beam. A sample-to-detector distance of 10 m was used to access

the q-range 0.0044-0.03 $Å^{-1}$. 2D scattering patterns were obtained using a Pilatus 2M detector. The 2D patterns for the hydrogel fiber with an initial solution concentration of 14.5 wt% in DMF are shown in Figure S4 below. No change in the domain spacing is evident (see Figure 4d of the manuscript), but there is a slight anisotropy evident in the samples between static and tensile configurations. The relative lack of anisotropy supports the hypothesis that the pores of these samples are deforming initially and control the mechanical properties at low extensions. At high strain, stress is gradually transferred to the polymer chains bridging the micelle cores, leading to eventual fracture. Up to moderate strain, as shown in Figure 4 of the main text and Figure S4 below, the nanostructure remains unchanged, with only a slight degree of anisotropy.

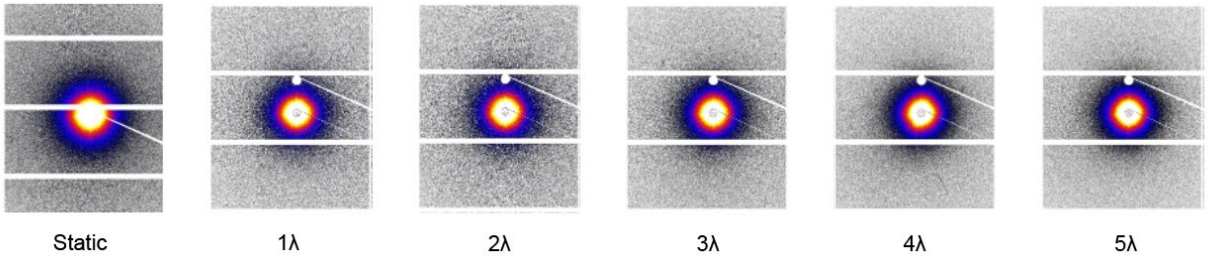

Figure S4. 2D scattering patterns of a THF 14.5 wt% hydrogel fiber at increasing extension. Minimal anisotropy occurring between static and tensile samples shows that the deformation of the gels up to moderate extension is dictated by the porous nanostructure rather than the micellar nanostructure.

6. Small-Angle Light Scattering Experiments

a. Experimental Setup

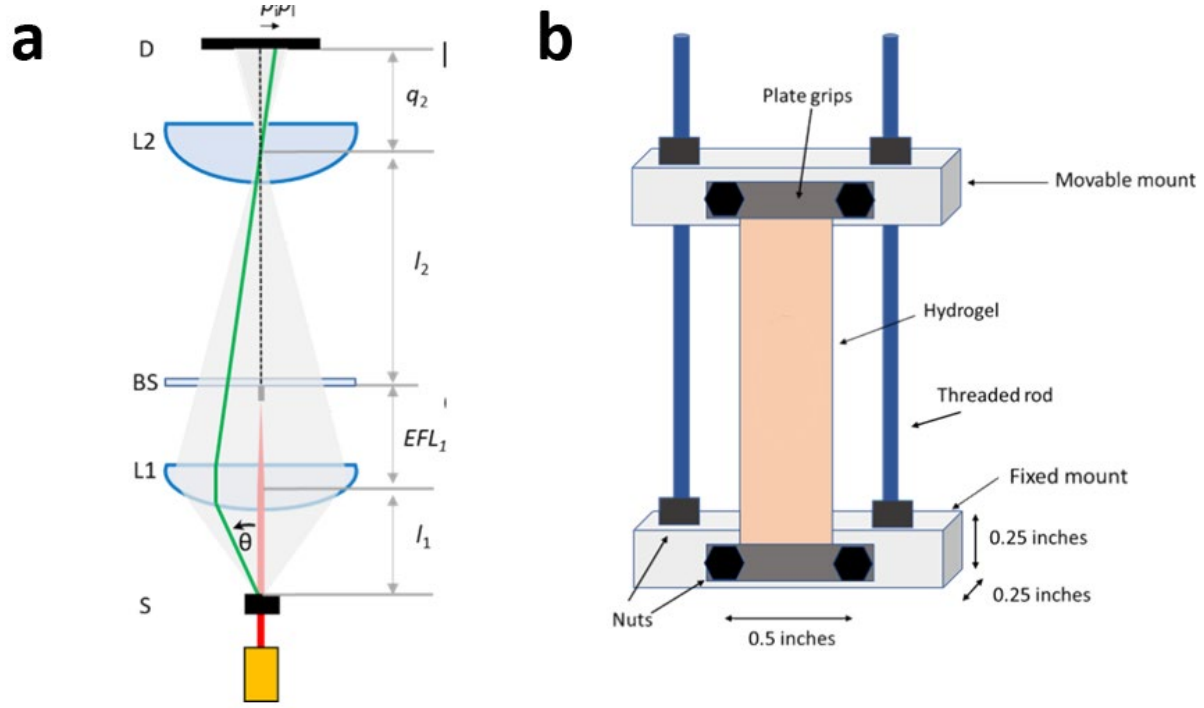

Figure S5. SALS experimental setup. a) Schematic diagram of the scattered light where S is the sample, θ is the scattering angle, focused by lens L1 through beamstop (BS) through lens L2 to a CMOS detector. b) Scheme of the stretching sample holder.

Figure S5a represents the small-angle light scattering (SALS) setup, which has been published previously.[5] The ray diagram shows the initial laser of 625 nm scattered from the sample at an angle θ through a convex lens L1 (Edmund Optics-NT67-245) with a numerical aperture, N.A. = 0.85 that captures up to 58° scattered light. The converging scattered light then passes through beam stop and is refocused through another convex lens L2 (Thorlabs-LA 1951A). The beam stop is at a focal length away from lens L1 and blocks all direct light from the laser. The l_1 and l_2 can

be changed to optimize the *q*-range. The scattered light is then projected onto a CMOS detector, D (Basler acA800-510 um) which is a focal length away from L2.

A control image is taken using a diffraction grating with 100 lines per mm. This was later used to determine the pixel-to-*q* conversion for the scattering patterns. The hydrogel was then loaded to the sample setup. The l_1 was set to ~25 mm and l_2 to ~75 mm. The room lights were then turned off to avoid any background scattering. A scattering image was then taken for each sample.

Figure S5b shows a schematic diagram of the sample setup. The hydrogel is held in the setup using plate grips. These plate grips are 0.5 in wide, offering enough space to load the hydrogel. The nuts can be moved allowing the top mount (movable) to move in z-direction. The hydrogel can then be stretched to different lengths.

b. Results under static and strained conditions

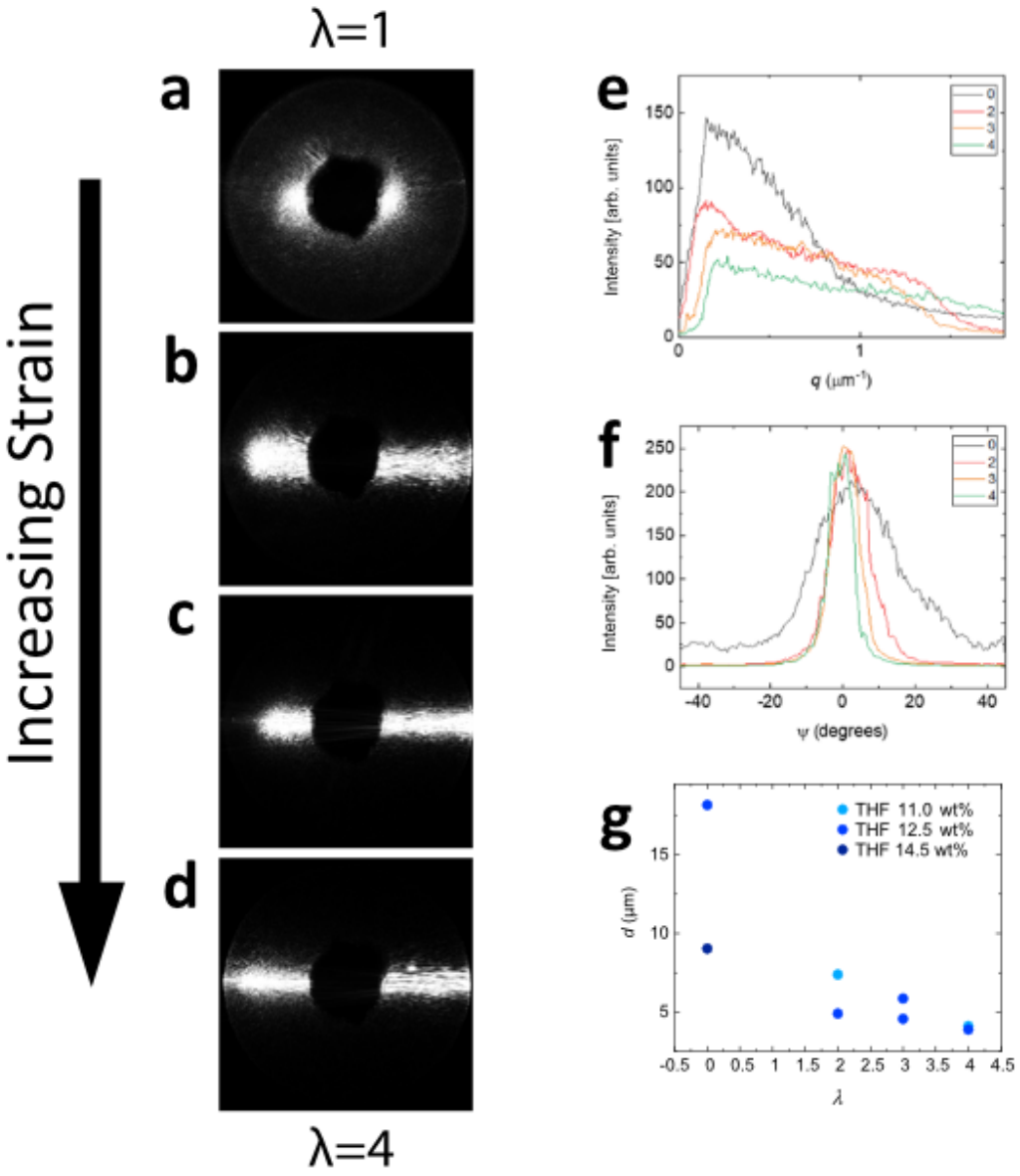

Figure S6. SALS data for a hydrogel prepared from a 12.5 wt% polymer solution in THF. 2D scattering plot for a) unstretched and stretched samples at elongation ratios of b) 2, c) 3, and d) 4. e) Intensity versus *q* plot at elongation ratios of 0, 2, 3, and 4. f) Intensity versus azimuthal angle, Ψ, plot at elongation ratios of 0, 2, 3, and 4. g) Pore domain spacing, *d*, as a function of elongation ratio for all tested samples produced using THF.

The hydrogel pore domain spacing, d, and alignment were determined from the 2D scattering plots shown in Figures S6a – d. The domain spacing for the unstretched sample was calculated to be ~ 20 μm in size using the equation, $d = 2\pi/q^*$, where q^* is the primary scattering peak from Figure S6e. The asymmetric 2D scattering plots indicate that the hydrogel pores are oriented along the long axis of the gels. As the sample is stretched, the scattering band widens perpendicular to the direction of stretch and decreases in intensity. Simultaneously, the orientation of the pore domains, which is along the fiber, increases, as seen from the narrowing of the scattering band and in the intensity versus azimuthal angle, Ψ, plot in Figure S6f. Furthermore, as the hydrogel is stretched, the in-plane distance between pores decreases from ~ 20 μm to 2-2.5 μm (Figure S6g). Full characterization of pore spacing for all samples at all elongation ratios was not possible for all samples due to the small size of samples.

7. Confocal Microscopy Images

Confocal measurements were performed on 5 mm sections of a fiber that had never been frozen, prepared using an initial solution concentration of 11.0 wt% polymer in THF and stained overnight in a 0.01 mg/mL solution of Nile Red in water. The samples were laid length-wise along the glass slide (Figure 7a) with a coverslip placed on top. The samples were imaged approximately parallel to the fiber axis at 10x (Figure S7b-d) and 63x magnification (Figure S7e-g), producing cross-sectional images showing the porous structure. The composite z-stack images at both magnifications (Figure 7d, g) show a high degree of alignment roughly parallel to the fiber axis, indicating an additional level of hierarchy potentially caused by the shear flow during injection.

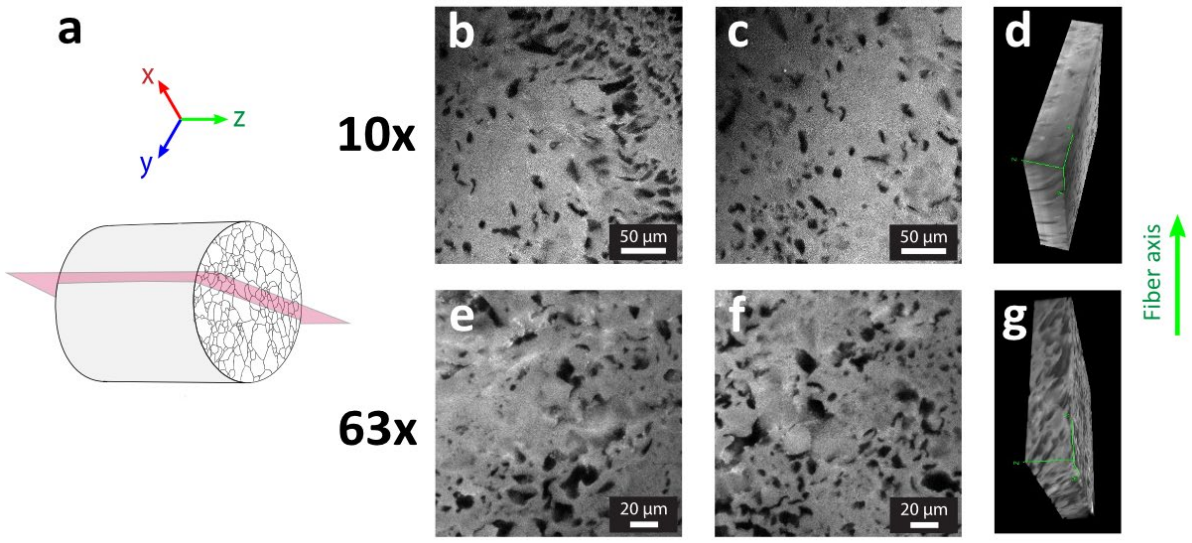

Figure S7. Confocal microscopy of a hydrated fiber produced using a 11.0 wt% polymer solution in THF. a) The cross-section orientation relative to fiber axis. b,c) 10x magnification of pores within the gel. d) Z-stack composite of 10x scans showing aligned pores. e,f) 63x magnification of pores within the gel. g) Z-stack composite of 63x scans showing aligned pores.

8. In situ transmission light microscopy (TLM) measurements

In situ TLM measurements (Figure 4d) were performed by combining a customized tensile tester with a confocal Raman microscope (Alpha 300R, WITec, Germany). The tensile tester was made using two linear piezo actuators (Physical Instrument, Germany) combined with L-shape clamps, allowing stretching of the samples while they were immersed underwater. The TLM images were captured using a 63X water immersion objective lens (Zeiss, Germany) while the sample was exposed to transmission white light. A strain rate of 0.5 mm/s was applied for stretching of the fibers, matching uniaxial extension tests.

9. Cryo-SEM imaging and Microstructure Analysis

a. *Sample Cross-Sections at Multiple Magnifications*

Imaging the fiber cross-sections was achieved by cutting the hydrogel fibers perpendicular to their length to produce 2 mm thick hydrogel discs. The sections were placed on the head of a 5 mm wide aluminum pin and placed in a cryo-microtome chamber cooled to -165 °C. After the discs had vitrified, the pins were mounted into clamps within the chamber and microtomed repeatedly until the height of the sample had been reduced by at least a half millimeter to ensure an accurate cross-section. The pins with the mounted samples were stored under liquid nitrogen. Samples were then transferred to a supercooled stud under liquid nitrogen, which was then transferred into the Cryo-SEM antechamber at -90 °C. The samples were sputter coated with a gold-palladium alloy, then transferred into the primary chamber for imaging.

Images of the hydrogel fibers are shown in Figures S8 – S13.

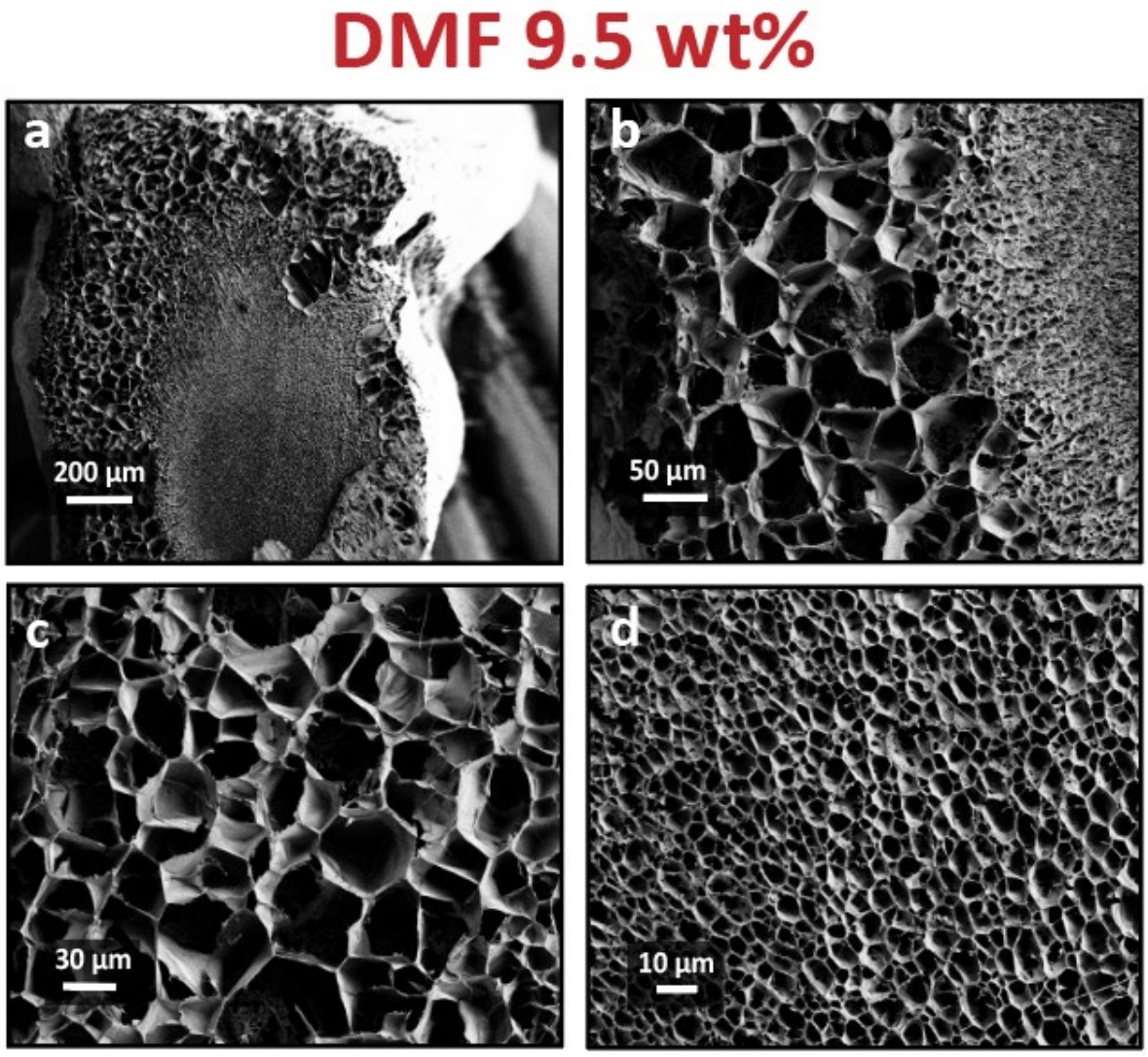

Figure S8. The cross-section of a vitrified hydrogel fiber, produced using a 9.5 wt% polymer solution in DMF, imaged using Cryo-SEM. a) The cross-section shows the coaxial structure with a high degree of variability in the thickness of the large pore outer sheath. b) Higher magnification of the fiber edge, showing the two distinct pore regions present in the fibers. c) High magnification of the large pore region. d) High magnification of the small pore region. Small pore region pores are much more uniform than large pore region pores.

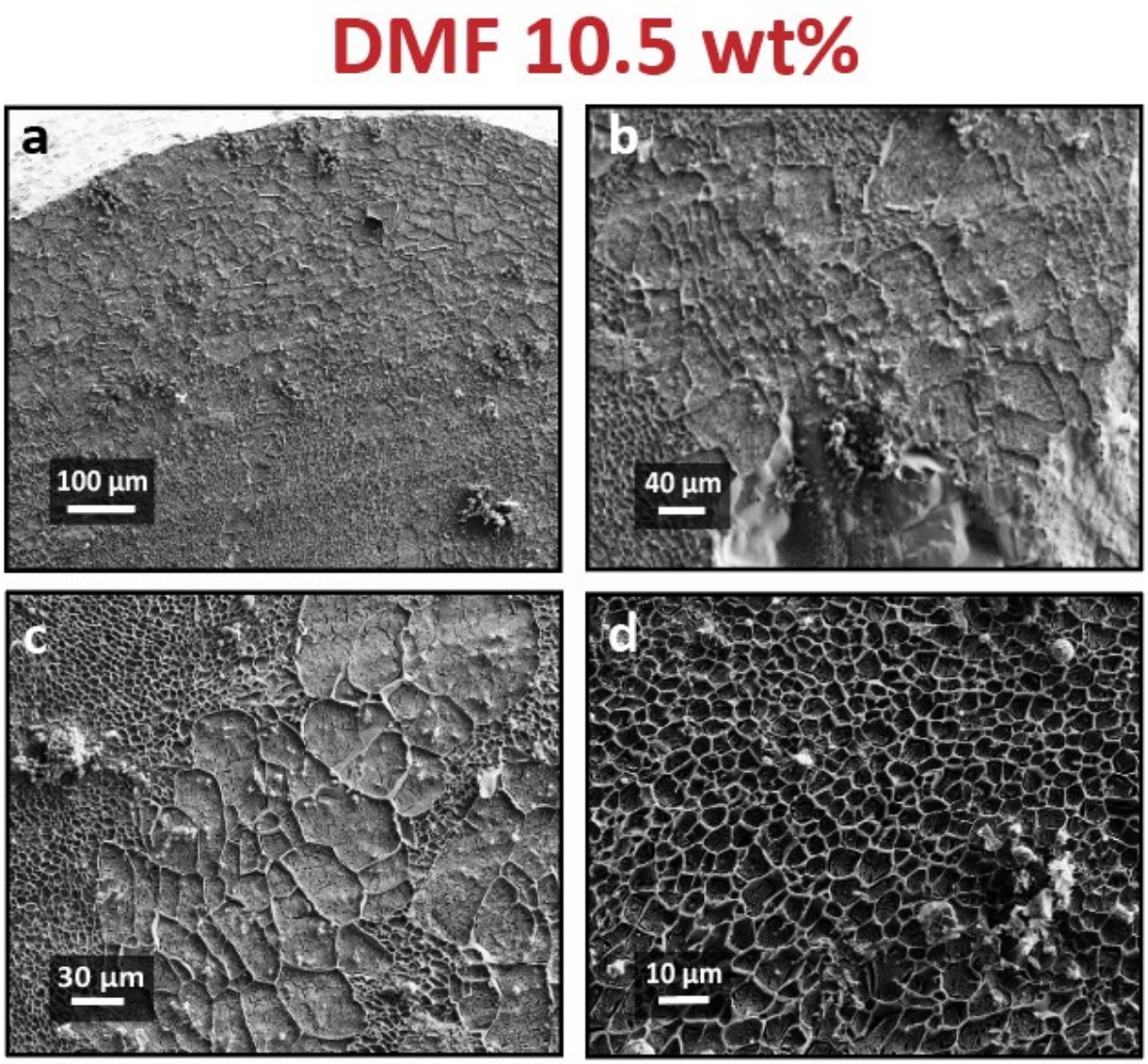

Fig S9. The cross-section of a vitrified hydrogel fiber, produced using a 10.5 wt% polymer solution in DMF, imaged using Cryo-SEM. Ice caps remained on large pores in the sample, reducing contrast. a) The cross-section shows the coaxial structure with less variability in the thickness of the large pore outer sheath. b) Higher magnification of the fiber edge, showing the two distinct pore regions present in the fibers. c) High magnification of the large pore outer region. d) High magnification of the small pore region.

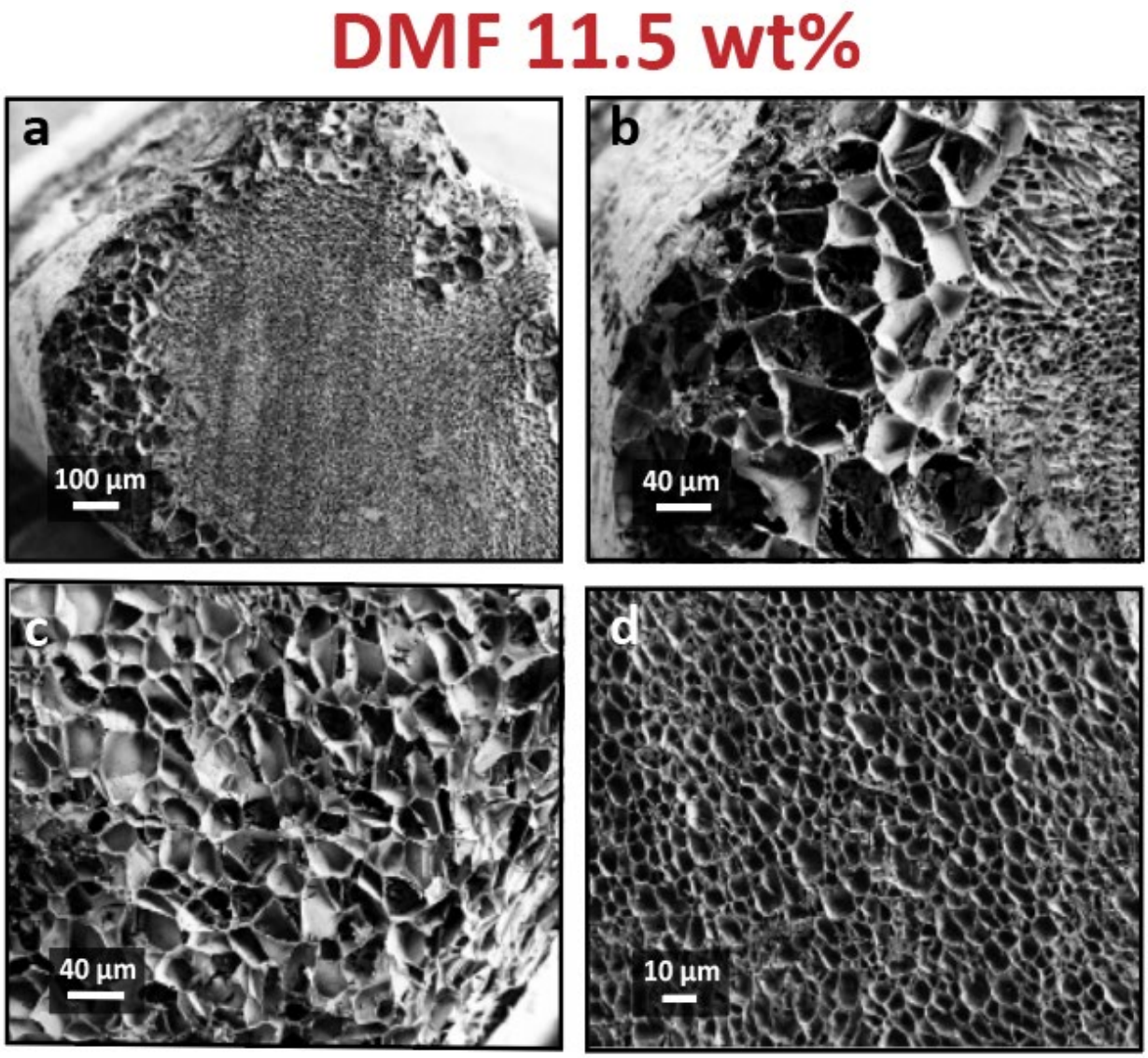

Fig S10. The cross-section of a vitrified hydrogel fiber, produced using a 11.5 wt% polymer solution in DMF, imaged using Cryo-SEM. a) The cross-section shows the coaxial structure is much more uniform, but the average value is well within standard deviation of the other two samples with this structure. b) Higher magnification of the fiber edge, showing the two distinct pore regions present in the fibers. c) High magnification of the large pore outer region. d) High magnification of the small pore region.

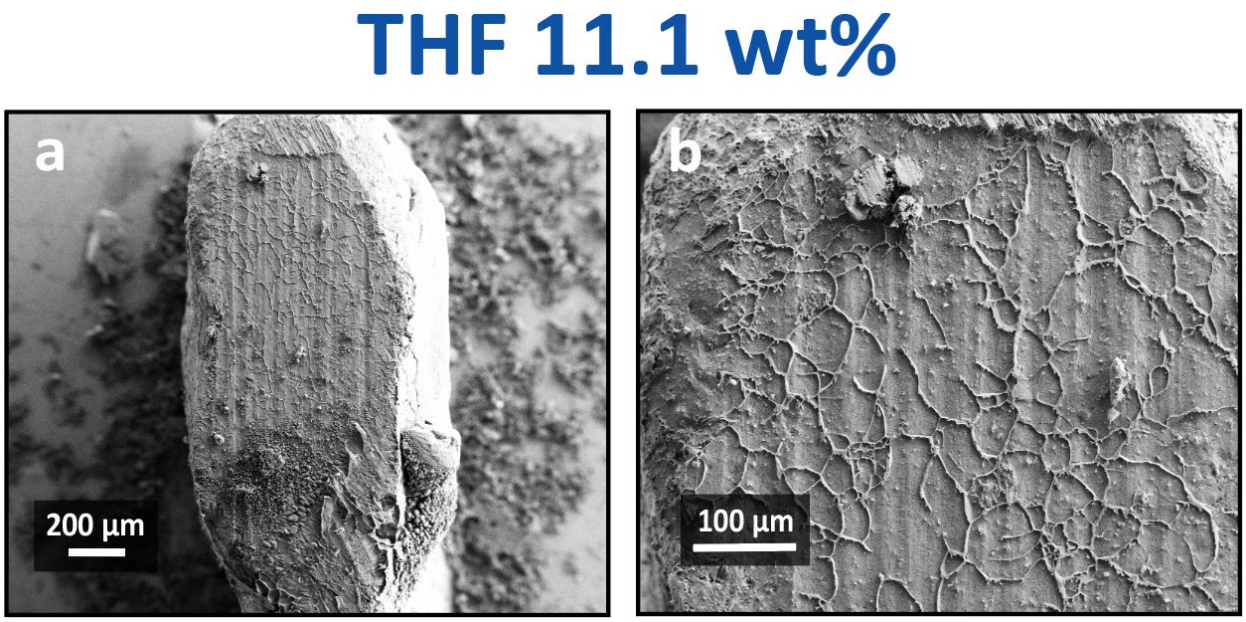

Fig S11. The cross-section of a vitrified hydrogel fiber, produced using a 11.1 wt% polymer solution in THF, imaged using Cryo-SEM. a) The fiber is primarily composed of a few large pores. b) Higher magnification image of the pores in this sample.

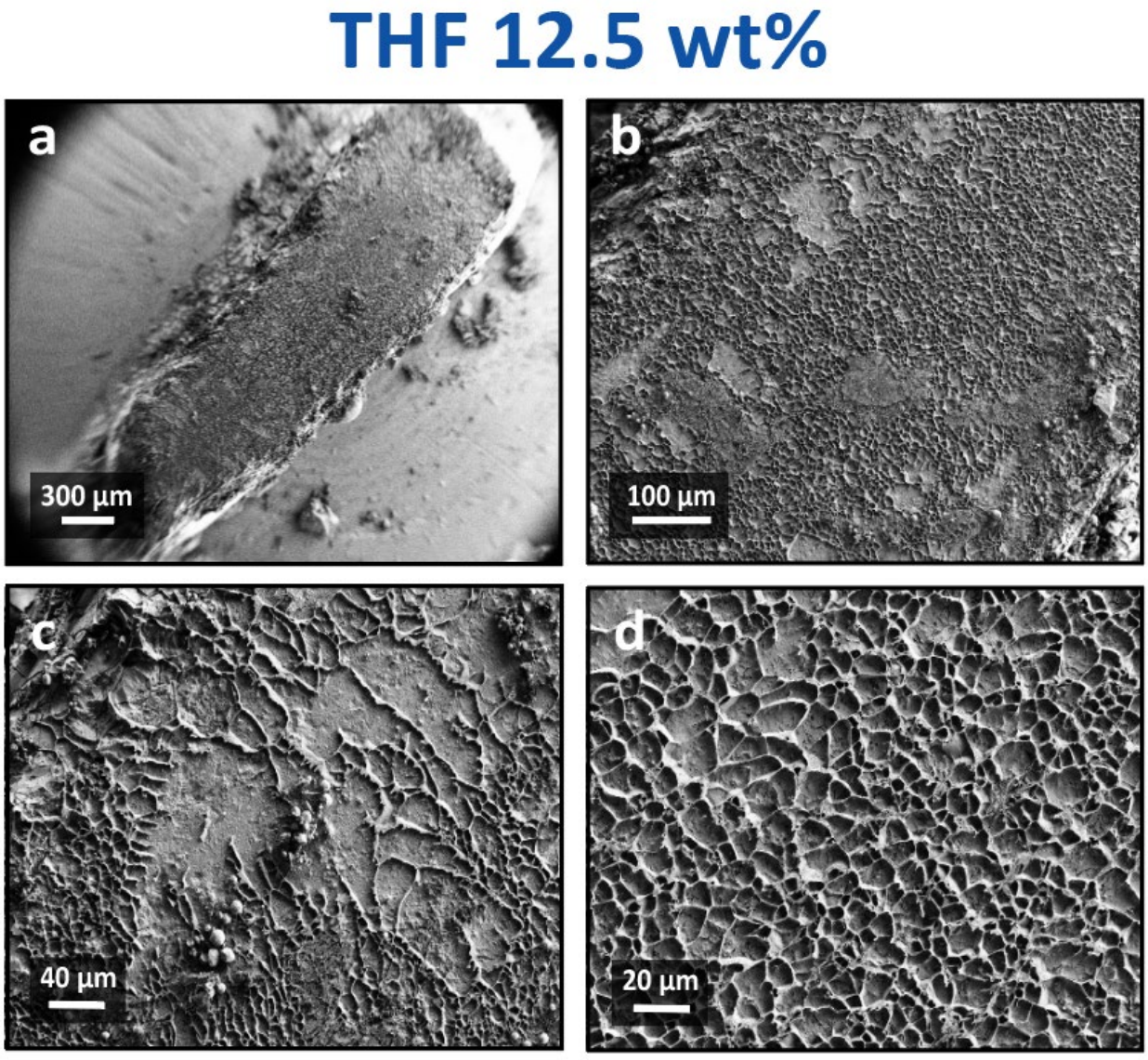

Fig S12. The cross-section of a vitrified hydrogel fiber, produced using a 12.5 wt% polymer solution in THF, imaged using Cryo-SEM. a) The fiber is primarily composed of a many small pores, with one lobe possessing an unusually high number of small pores. b) Large pores were also scattered sporadically throughout the sample, with c) clear boundaries between the two. d) The small pore region in this sample. All small pore regions imaged in this study showed a high degree of uniformity as well as a striking similarity in size distribution with one another.

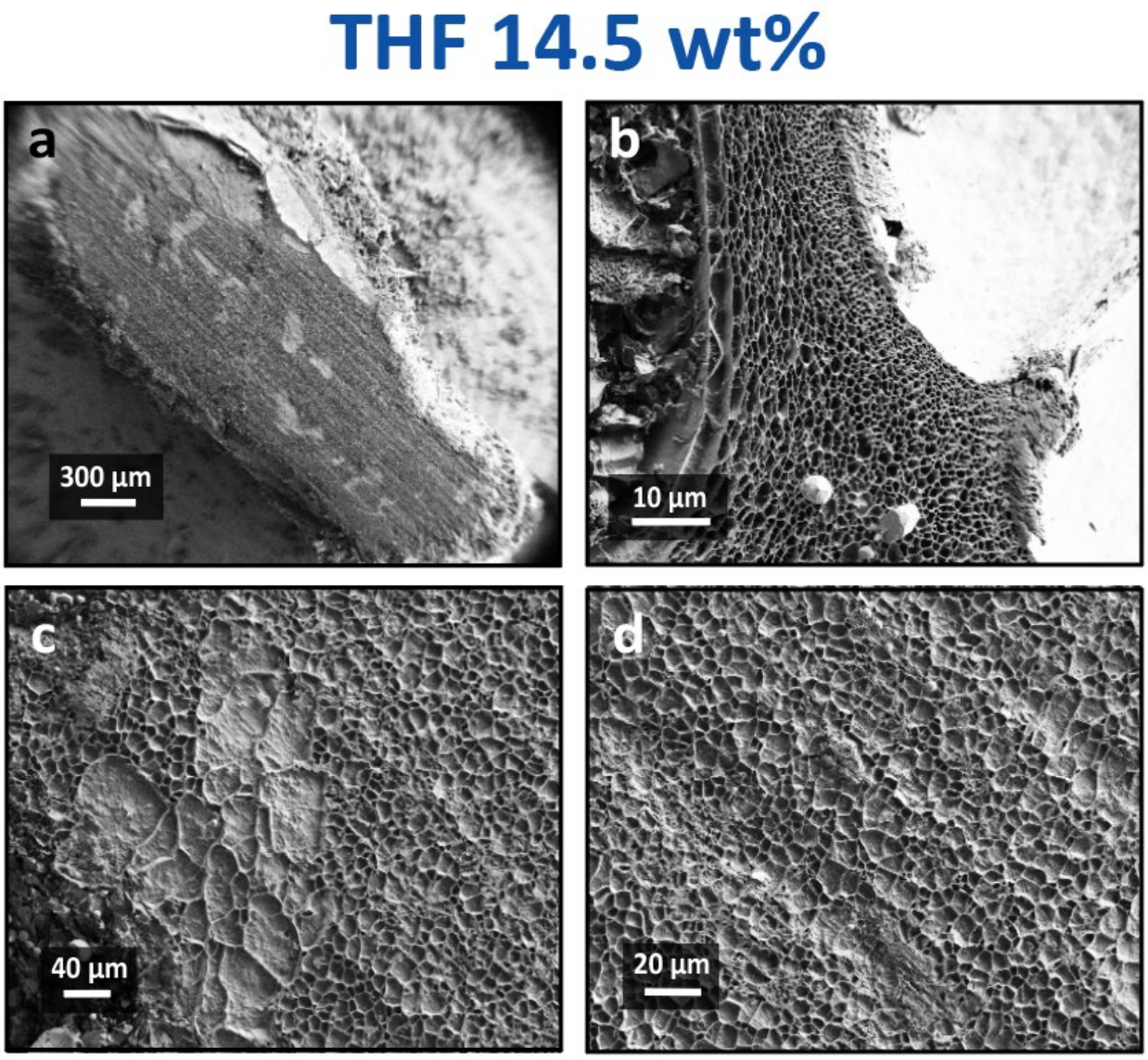

Fig S13. The cross-section of a vitrified hydrogel fiber, produced using a 14.5 wt% polymer solution in THF, imaged using Cryo-SEM. a) The fiber is almost entirely composed of many small pores, with a few sporadic large pores. b) Edge of bubble inclusion withing the fibers, where the pores compressed between the bubbles appeared much stronger. This may indicate a role shear force plays in determining pore size. c) Clear boundaries between the large and d) small pores.

b. *Micrograph Analysis using ImageJ Software*

Pore sizes for the hydrogel samples were determined from cryo-SEM images that were analyzed via ImageJ software downloaded from nih.gov. First, cryo-SEM images were despeckled and converted to 8-bit binary. Then, the image threshold was set so that the pores were black regions bounded by white pore walls (Figure S14). Spot analysis with a minimum area of 1 μm^2 was used to eliminate static still caught within the threshold to produce measurements of the total area and Feret Diameters (the largest length between two pore walls) of each pore in the image. Some images exhibit poor contrast, and thus, the analysis was done by hand.

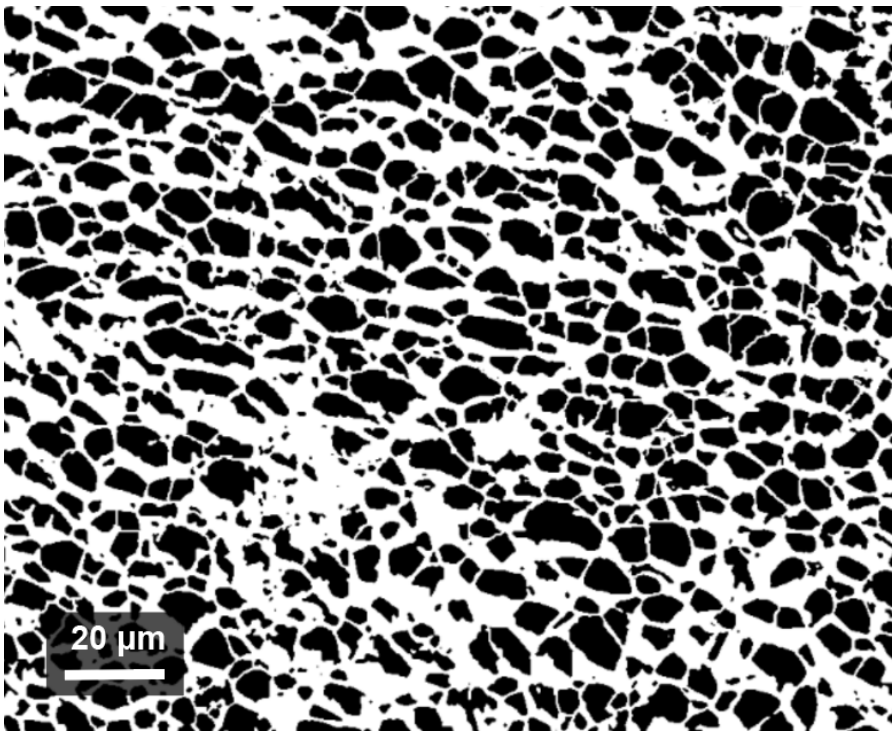

Figure S14. Pore image after being smoothed and converted to 8-bit binary via ImageJ software. A spot analysis with a minimum area of 1 μm^2 is used to calculate the average pore size.

Small Pore Area Fraction

A rough estimate of the fraction of the cross-section area comprised of small pores was obtained by dividing the total area of the hydrogel fiber cross-section, determined using ImageJ, by the area of the small pore regions, calculated by the method described in the previous section. These values were confirmed by measuring the large pore area and performing the same calculation.

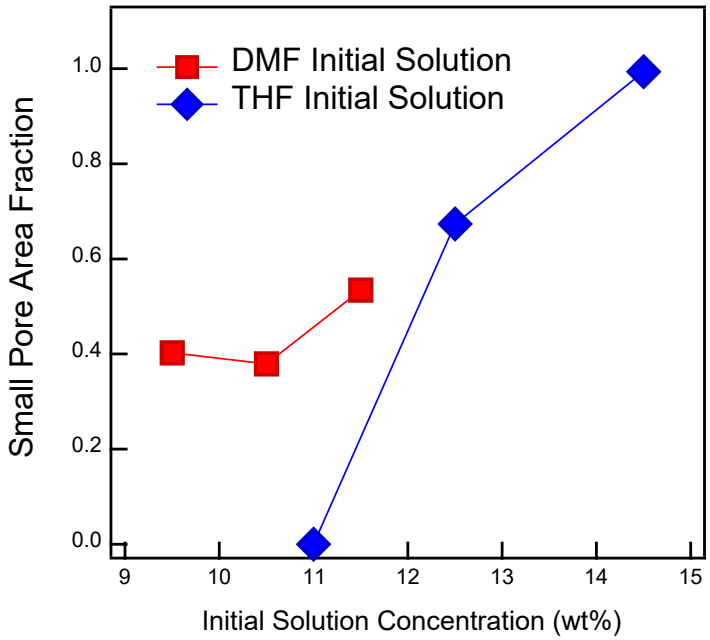

Figure S15. The fraction of the fiber area comprised of small pores for samples produced using DMF (red) and THF (blue) as the initial organic solvents. The small pore area fraction remains relatively consistent for the DMF samples but increases dramatically for the THF samples. The bubble inclusions in the hydrogel fiber cross-sections were not included in the calculation for the sample produced using an initial polymer solution concentration of 14.5 wt% in THF.

Characterization of the Core-Sheath Morphology

The relative thickness of the outer "sheath" large-pore region in fibers possessing the coaxial morphology was measured perpendicular to the edge of the fiber at points equidistant along the perimeter of the fiber sample in Image J. As concentration increases, the diameter of the "sheath" region appears to decrease but is within error (Figure S16). It is possible that this indicates a trend, the existence of which is further supported by the increase in small pore area fraction seen in this morphology (see Figure S15). However, because variations are within error for the concentrations accessible in this study, no further conclusions may be drawn at this time.

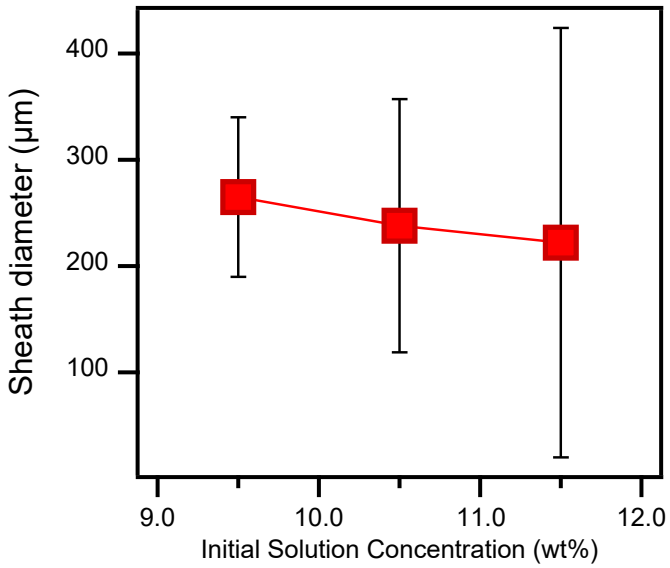

Figure S16. A slight decrease in the thickness of the large pore "sheath" region is observed from the hydrogel cross-section micrographs for DMF samples. However, the variations are within error of one another, and the potential for other parameters to affect morphology effectively prevents any conclusions from being drawn from the data at this time. Sheath diameters for all samples are represented as mean values with error bars representing standard deviation. The number of replicate measurements are n = 3, 28, and 41 for DMF samples 9.5 wt%, 10.5 wt%, and 11.5 wt%, respectively.

10. Solvent Diffusion Coefficients Measured by Tracer Diffusion Experiments

The polymer solution viscosity was held constant between two samples — THF 11.0 wt% and DMF 11.5 wt% — to isolate the effect of varying the solvent used to prepare the hydrogel. As seen in Figure S2b, the viscosity of the initial DMF and THF polymers solutions are in the same range, indicating that the polymer solution viscosity should have the same effect in both DMF and THF. Contrary to these expectations, the cryo-SEM images in Figure 3a-d in the manuscript show that the microstructures of the hydrogels are drastically different; THF and DMF exhibit either entirely large pores or the coaxial fiber structure, respectively.

To assess the impact of solvent diffusion, we incorporated 1 mg/mL of Eosin Y disodium salt into the initial solvents to trace the diffusion of the solvent out of solution. Briefly, 0.1 mL of the solvent/polymer/EY solutions were placed in the bottom of a quartz cuvette. At t = 0, 3 mL of water were added to the cuvette, and the increase in the maximum intensity of the EY peak was plotted with respect to time and fitted with Fick's 2nd Law of Diffusion to determine the diffusion coefficient (Figure S17). Interestingly, the values were highly consistent at 0.036 ± 0.0075 cm^2/min across solvent, polymer concentrations, and tracer concentrations, indicating that the diffusion of the solvent is determined by the gel rather than the solvent.

Tracer diffusion experiments using Eosin Y disodium salt (EY) were conducted to compare solvent diffusion coefficients between THF and DMF during hydrogel formation by tracking the increase in EY concentration during solvent exchange. Figure S17a shows that the EY absorption increases with time, as expected, and Figure S17b shows the plot of the normalized maximum absorption for solutions with respect to time. The experimental data was fitted with Fick's Second Law of Diffusion to quantify the diffusion coefficient. Interestingly, the solvent exchange rate between THF and DMF are within error, indicating that the solvent exchange rates are the same

between the two solvents. The calculated EY diffusion coefficient was constant at or around 0.036 ± 0.0075 cm^2/min for all initial polymer solution concentrations used in the study. Additionally, the diffusion coefficient does not show significant change when concentration of the tracer is increased, while keeping other parameters the same. Thus, solvent exchange rate is predicted to play a minimal role in dictating the hydrogel microstructure.

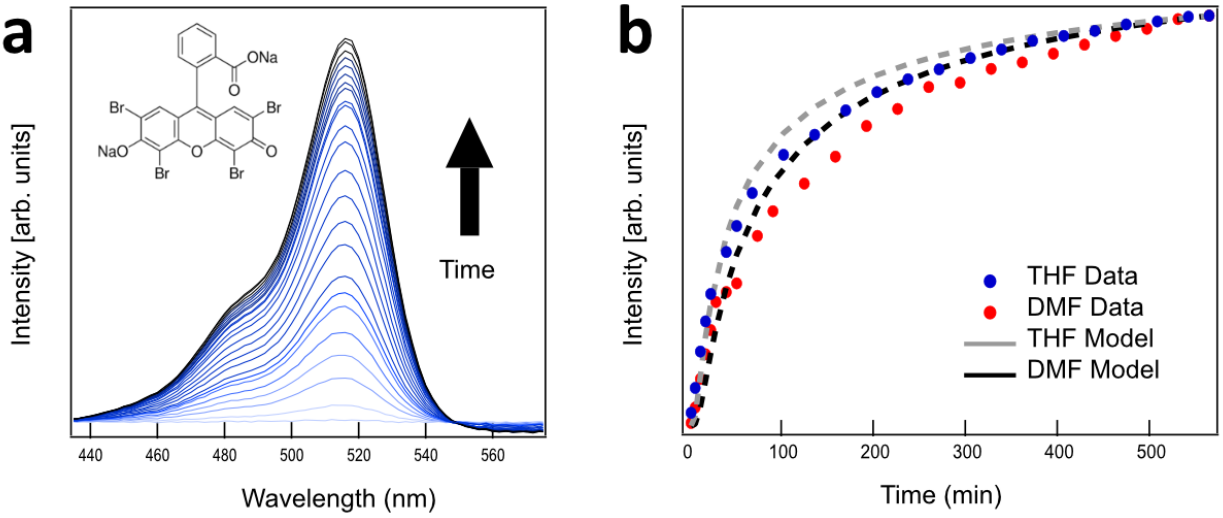

Figure S17. Measuring EY absorbance during solvent exchange. a) EY absorbance increases with time as EY diffuses out of the hydrogel. b) Plot of normalized intensity vs. time (min), where t = 0 is the point at which water was added to the cuvette containing the solution of EY, solvent, and polymer. The data was fit with Fick's 2nd Law of diffusion to calculate the diffusion coefficient of the solvent as it diffuses from the gel.

11. Critical Water Content Measurements

The critical water content (CWC) — i.e., the fraction of water that induces micellization in the block copolymers — was calculated by measuring the scattering intensity of filtered, dilute solutions of the triblock copolymers in THF and DMF as the weight fraction of water in solution increased. Measurements were conducted using a Brookhaven Instruments BI-200SM Research goniometer system with a 637 nm, 30 mW laser and a 100 µm aperture, and the solutions were filtered twice using a 0.45 µm Teflon filter. The concentration of the initial THF and DMF solutions was selected to be 4 and 2.5 mg/mL through trial and error as the lowest concentrations producing measurable scattering. As shown in Figure S18, the critical water content is identical for both THF and DMF solutions, where onset and completion of micellization occurs between 7-8% water by weight. This value was shown to be unaffected by concentration.

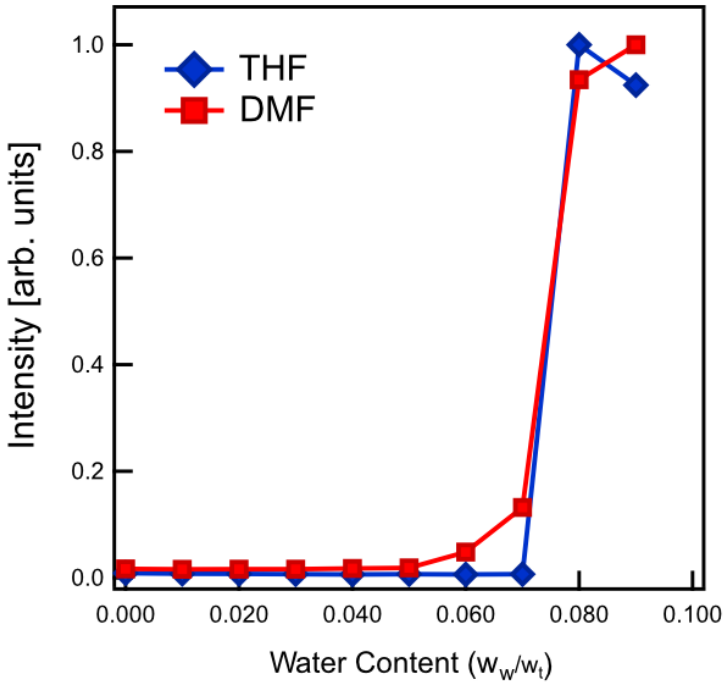

Figure S18. Critical water content measurements in a dilute triblock copolymer solution in THF and DMF.

12. Mechanical properties

a. *Measuring fiber cross-sectional area*

The low modulus and tensile strength of these hydrogels required a precise measurement of the cross-sectional area to accurately calculate the applied stress. Due to irregularities in the shape of the hydrogel fibers, the area was determined by taking cross-sectional slices of the hydrogel — similar to those mounted on aluminum pins for cryo-microtoming — and examining them under a bright field microscope at 2.5x magnification. Measurements were performed quickly, as the heat of the microscope began to evaporate the water withing the hydrogels. At least five representative slices were used for each cross-section, and the area of the cross-sections was calculated using Image J.

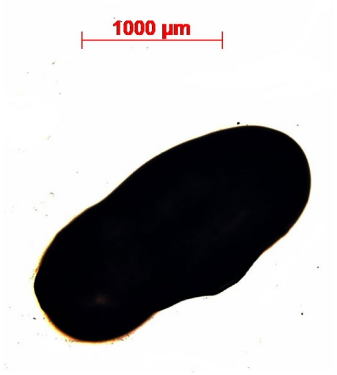

Figure S19. Example hydrogel slice used to calculate cross-sectional area for fiber samples. Images were obtained with a bright field microscope at 2.5x magnification.

b. Summary of calculated values

Due to the noise in the data, the Young's Modulus (E) was calculated from a trendline fit to the first 100 points of data for every sample tested. The tensile strength corresponds with the maximum stress achieved by the samples. The toughness was calculated from the area under the stress-strain curve. Values are averaged for 5 to 7 samples per sample concentration. Average values and raw data are shown below.

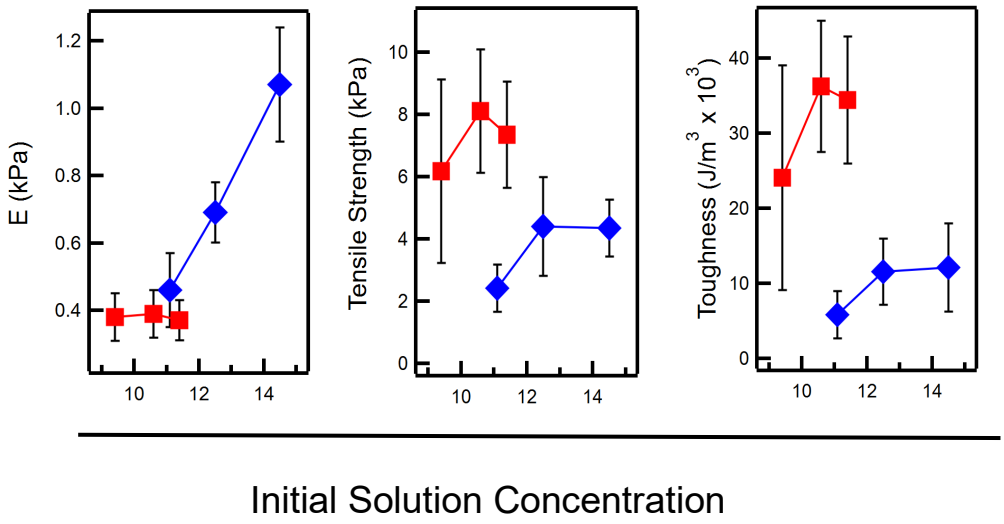

Figure S20. Summary of measured mechanical properties. The Young's Modulus for the DMF samples was highly consistent as the initial polymer solution increased, but the samples made with THF show a steady increase in *E* with concentration. The tensile strength of the samples produced with DMF were unchanging within error of one another, while the THF samples showed an increase. The variability in DMF sample tensile strength is reflected in the values calculated for toughness, but once again the values are all within error of each other. The THF samples show little variation in toughness due to the decrease in elongation with increasing initial solution concentration (see Figure 4a in the manuscript). Young's Modulus, tensile strength, and toughness values determined from uniaxial extension measurements are represented as mean values with

error bars representing standard deviation. The number of replicate uniaxial extension measurements (n) for DMF are n = 8, n = 12, and n = 7 for 9.5 wt%, 10.5 wt%, and 11.5 wt%, respectively. THF samples with mean values and error bars are n = 10, n = 5, and n = 8 for 11.0 wt%, 12.5 wt%, and 14.5 wt%, respectively.

c. Raw data for uniaxial extension tests

Uniaxial extension tests were performed using spring-loaded steel grips and a 10 N load transducer on a Criterion Load frame from MTS. All samples were deformed at a rate of 3/min. In the graphs shown below, the sample data for a given initial solution condition is shown in gray, with the representative trace, which had the closest alignment to the average elongation ratio and ultimate tensile strength at break for each sample condition, highlighted in color. The color used corresponds with the samples shown in Figure 4a in the manuscript. The data for samples produced with DMF as the organic solvent shows a high degree of variability in the elongation at break at lower initial polymer solution concentrations, with some fibers failing earlier (6 times original length). Though the cause of this is unclear, it may potentially be attributed to slightly larger outer pore regions allowing cracks to propagate more easily. As initial polymer solution concentration increases for the samples produced using DMF, the elongation at break and ultimate tensile strength of the hydrogels becomes more consistent. Dips and drops in the data are attributed either to slight tearing of the fiber or to observed slippage of the hydrogel fiber from between the clamps.

THF samples showed distinct trends in mechanical properties with increasing concentration: as concentration increased, so did tensile strength and elastic modulus, consistent

with results reported in previous publications where THF was used as the organic solvent. Conversely, the elongation at break decreased with increasing initial solution concentration.

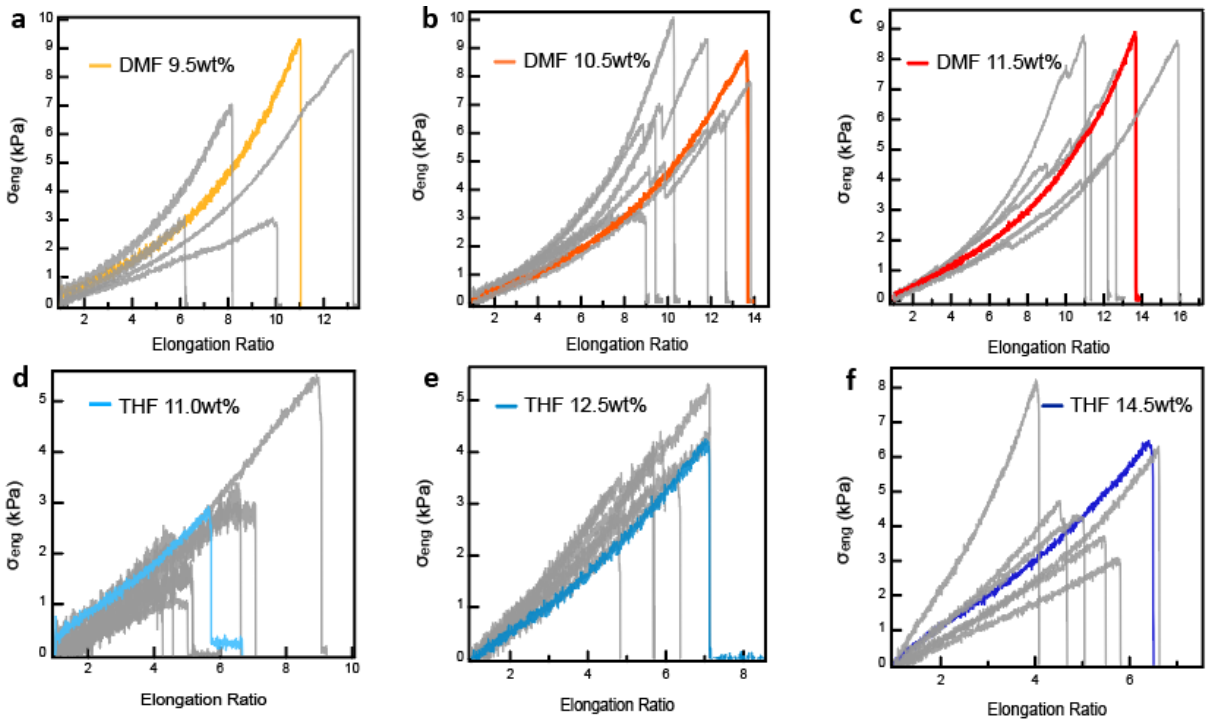

Figure S21. Stress-strain curves generated from uniaxial tensile tests for hydrogel fibers. Representative samples are shown in color for a) DMF 9.5 wt%, b) DMF 10.5 wt%, c) DMF 11.5 wt%, d) THF 11 wt%, e) THF 12.5 wt%, and f) THF 14.5 wt%. A minimum of four samples were tested for each sample condition. Though DMF samples showed greater variability in mechanical properties (ultimate tensile rate) at low initial solution conditions, the average values remained consistent. In contrast, samples prepared with THF increase in both average modulus and tensile strength with concentration, but elongation at break decreases with increasing concentration.

13. Oscillatory shear rheology on hydrogels

While the injected fiber samples were amenable to uniaxial extension tests, the hydrogels produced using conventional methods were brittle. The shear modulus of these hydrogels was measured via oscillatory shear rheology using a TA Ares-G2 rheometer, first with a dynamic strain sweep to determine the strain region appropriate for testing, and next with a dynamic frequency sweep from 0.1-10 rad/s. Interestingly, the hydrogel fibers showed no change in the storage modulus *G'* with solvent or initial strain, as the storage modulus was approximately equal at both 10 and 100% strain. In contrast, the annealed "equilibrium" sample could only be tested at a strain of 2%. The lack of difference between samples is most likely due to the consistent swelling ratio for all samples.

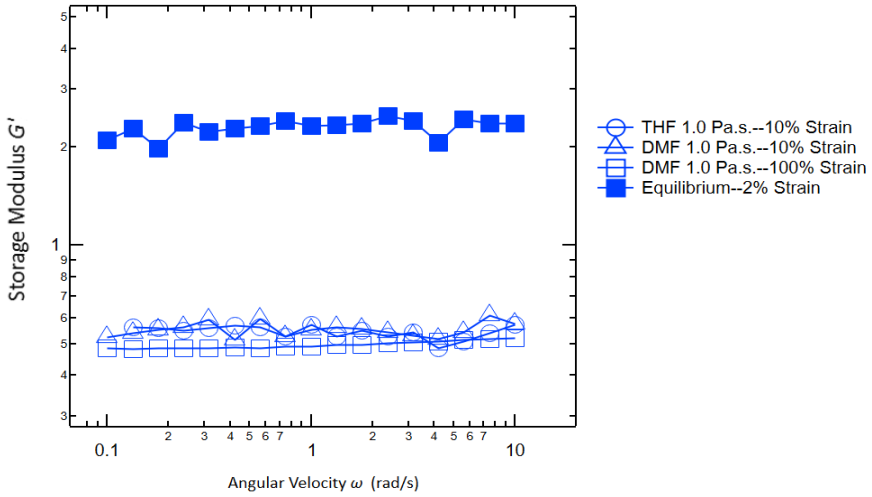

Figure S22. Oscillatory shear rheology measurements for conventional samples and injected fiber hydrogel samples. Samples prepared through conventional methods were brittle and were thus tested at low strain. The shear modulus of the hydrogel samples was five times greater in the conventional samples than in the injected fiber samples, which is consistent with expectations. Interestingly, the injected fiber samples showed a consistent storage modulus, despite variations in both samples and strain.

14. Property Comparison with Hydrogels in the Literature

Table S2: Reported values from the literature for maximum tensile strength, Young's Modulus, and elongation ratio at break for physical, single network, interpenetrating network, supramolecular, and porous gels. Values not reported are indicated by "NR," and values with an asterisk were tested under compression. Reported values plotted with permission in Figure 4f of the manuscript.

Hydrogel Class	σ_{max} (MPa)	E (MPa)	λ_b	Reference in Manuscript
Physical Gel	1.5-5	0.2-5	2.2-3.5	*33*
Physical Gel	1-7.5	5	4.5-5.0	*35*
Physical Gel	0.004-0.43	NR	1.4	*18*
Physical Gel	20-200	NR	8.0	*34*
Single Network	2.5-5	2-20	3.5-5	*11*
Single Network	0.4-4	0.01-0.04	2.0-1.9	*10*
Single Network	0.025-0.4	0.001-2	2.0-8.0	*12*
Single Network	0.035-0.7	0.0184-0.072	5.0-8.0	*4*
Single Network	1-9	0.114-10	2.0	*13*
Interpenetrating Network Gel	50-250	0.008-0.374	1.25-5.0	*48*
Interpenetrating Network Gel	2.1-3.1	0.5-6.5	4.0-9.0	*49*
Interpenetrating Network Gel	0.1-17.2	NR	7.0	*50*

Hydrogel Class	σ_{max} (MPa)	E (MPa)	λ_b	Reference in Manuscript
Supramolecular	0.5-6	NR	11-15	*45*
Supramolecular	0.01-0.052	NR	15-33	*44*
Supramolecular	0.75-2.5	NR	11-21	*46*
Porous	0.014-0.21*	NR	1.25-1.63*	*40*
Porous	0.005-0.014*	NR	1.15*	*16*
Porous	0.025-0.15*	0.96-5.8	1.6*	*37*
Porous	0.12*	0.0073	1.95*	*38*
Porous	0.0025-0.015*	0.0015-0.023	1.5*	*39*

Supplementary References

1. Lang C, LaNasa JA, Utomo N, Xu Y, Nelson MJ, Song W*, et al.* Solvent-non-solvent rapid-injection for preparing nanostructured materials from micelles to hydrogels. *Nat Commun* 2019, **10:** 3855.

2. Hillmyer MA, Bates FS. Synthesis and Characterization of Model Polyalkane−Poly(ethylene oxide) Block Copolymers. *Macromolecules* 1996, **29**(22)**:** 6994-7002.

3. Merrill BA. Potassium Naphthalenide. *Encyclopedia of Reagents for Organic Synthesis*. John Wiley & Sons, 2001.

4. Guo C, Bailey TS. Highly distensible nanostructured elastic hydrogels from AB diblock and ABA triblock copolymer melt blends. *Soft Matter* 2010, **6**(19)**:** 4807-4818.

5. Dhakal S, Chen Z, Estrin D, Morozova S. Spatially-Resolved Network Dynamics of Poly(vinyl alcohol) Gels Measured with Dynamic Small Angle Light Scattering. *Gels* 2022, **8**(7)**:** 394.